R-09-32

System and safety studies of accelerator driven systems for transmutation

Annual report 2008

Vasily Arzhanov, Calle Berglöf, Andrei Fokau
Mikael Jolkkonen, Odd Runevall, Nils Sandberg
Milan Tesinsky, Janne Wallenius and Youpeng Zhang

Division of Reactor Physics
Royal Institute of Technology

July 2009

Svensk Kärnbränslehantering AB
Swedish Nuclear Fuel
and Waste Management Co

Box 250, SE-101 24 Stockholm
Phone +46 8 459 84 00

SKB

ISSN 1402-3091
SKB Rapport R-09-32

System and safety studies of accelerator driven systems for transmutation

Annual report 2008

Vasily Arzhanov, Calle Berglöf, Andrei Fokau
Mikael Jolkkonen, Odd Runevall, Nils Sandberg
Milan Tesinsky, Janne Wallenius and Youpeng Zhang

Division of Reactor Physics
Royal Institute of Technology

July 2009

Summary

Within the project “System and safety studies of accelerator driven systems for transmutation”, research on design and safety of sub-critical reactors for recycling of minor actinides is performed. During 2008, the reactor physics division at KTH has made a design study of a source efficient ADS with nitride fuel, based on the EFIT design made within the EUROTRANS project. Transient analysis for EFIT-400 ADS with cercer and cermet fuels was made with SAS4A, taking into account flow reversal phenomena. Using Pulsed Neutron Source techniques, reference reactivity values for detectors in the sub-critical YALINA booster facility were obtained and it was observed that the results carry strong spatial effects. It was shown that the beam trip technique can be used to obtain the reactivity at beam trips and the values can be used for calibration of a current-to-flux reactivity indicator. Multi-scale modelling of helium desorption from moleybdenum was performed, with the final aim to predict the in-pile behaviour of Mo based CERMET fuel. Good agreement with experimental data was obtained, except at the highest temperatures.

Sammanfattning

I projektet ”System- och säkerhetsstudier av acceleratordrivna system för transmutation” utförs forskning om design och säkerhet för underkritiska reaktorer avsedda att förbränna mindre aktinider. Under 2008 har avdelningen för reaktorfysik på KTH utformat en källeffektiv ADS med nitridbränsle, baserad på den EFIT-design som tagits fram i EUROTRANS-projektet. Transientanalys för EFIT-400 med cercer och cermetbränsle har utförts, med hänsyn tagen till vändning av kylmedelsflöde. Reaktivitetsvärden för detektorer i YALINA-booster har uppmätts med pulserande neutronkälleteknik, varvid ett tydligt rumsberoende noterades. Dessutom har vi visat att strålavbrott kan användas som en teknik för att mäta reaktivitet och att dessa värden kan användas för att kalibrera ström/flödesindikatorer för reaktivitet. Flerskalemodellering av heliumavgivning från molybden utfördes med slutmål att kunna förutse beteendet hos molybdenbaserat CERMET-bränsle under bestrålning. Beräkningarna stämmer väl överens med experimentella data, utom vid de allra högsta temperaturerna.

Contents

1	**Introduction**	7
2	**Safety studies of ADS and Gen-IV systems**	9
2.1	Neutronic analysis	9
	2.1.1 CERCER fuel	9
	2.1.2 CERMET fuel	9
	2.1.3 Nitride fuel	9
	2.1.4 Nuclear data issue	9
	2.1.5 Nitride fuel reactivity swing and power profile	10
2.2	Transient analysis	10
	2.2.1 Unprotected Loss of Flow (ULOF)	10
	2.2.2 Unprotected over Power (UTOP)	10
	2.2.3 Modelling of flow reversal	11
	2.2.4 Limits to americium concentration in critical fast neutron reactors	12
2.3	Source term	12
3	**Sub-criticality monitoring**	13
3.1	Experimental set-up	13
3.2	Pulse neutron source experiments	14
	3.2.1 Prompt decay constant method	14
	3.2.2 Area method	15
	3.2.3 Beam-Trip Measurements	16
	3.2.4 Conclusions	16
3.3	Neutron detection at YALINA-booster	17
3.4	Deviations from point kinetics	18
4	**Fuel modelling**	21
4.1	Introduction	21
4.2	Methodology	21
4.3	Results	22
4.4	Conclusions	23
4.5	Fuel laboratory	23
5	**Modelling of radiation damage in steels**	25
6	**References**	27
7	**List of publications**	29
8	**List of participation in conferences and project meetings**	31

1 Introduction

Research on accelerator driven systems (ADS) for transmutation of nuclear waste is performed at the division of reactor physics at KTH. Presently, the major context of this research is the EUROTRANS project in the 6th framework programme of the European Commission, where design of an experimental ADS with MOX fuel and lead-bismuth coolant (XT-ADS) and an industrial demonstration facility for minor actinide transmutation (EFIT) is made. Development of ADS fuel and structural materials are integrated into the project.

The division of reactor physics at KTH is participating in all domains of the EUROTRANS project, in particular with the following activities:

Domain DESIGN:	Co-ordination of the safety work package. Assessment of the source term in case of severe accidents.
Domain ECATS:	Development and testing of methods for sub-criticality monitoring.
Domain AFTRA:	Fuel modelling, Transient safety analysis.
Domain DEMETRA:	Modelling of radiation damage in Fe-Cr-C steels.

Furthermore, KTH participated in the ELSY, PUMA and GETMAT projects, where development of fast neutron lead cooled reactors (ELSY), high temperature gas cooled reactors (PUMA) and structural materials for Gen-IV and ADS systems (GETMAT) are developed, all in the general context of minor actinide transmutation.

In the present report, a summary of activities performed at KTH during 2008 is provided, including an account for participation in conferences and project meetings.

2 Safety studies of ADS and Gen-IV systems

2.1 Neutronic analysis

During 2008, one of the main research topics was an optimization of the first industrial ADS (EFIT) design in respect of source efficiency and transmutation performance. Three fuel candidates (namely, CERCER, CERMET and nitride fuel) were studied with corresponding design adjustments.

2.1.1 CERCER fuel

In Domain 1 (DESIGN) of the Integrated Project EUROTRANS, oxide fuel with MgO matrix (CERCER) was chosen as the primary fuel candidate. The main advantage of MgO is its low neutron capture rate, leading to core designs with relatively high transmutation performance.

2.1.2 CERMET fuel

In Domain 3 'AFTRA' of EUROTRANS, an alternative solution of ADS fuel with Molybdenum matrix (CERMET) and corresponding core design are developed (Figure 2-1). Mo based CERMET fuel offers enhanced safety features and better high temperature stability as compared to MgO based CERC fuel.

2.1.3 Nitride fuel

Nitride fuel has been in focus of transmutation research already two decades. The concept of nitride fueled ADS is developed by KTH and traditionally by Japanese research institutions. During 2008, a design of highly source efficient ADS has been proposed and studied (Figure 2-1). It was found that utilization of nitride fuel and austenitic steel cladding allows to design ADS with higher average neutron energy (i.e. higher fission probability for minor actinides), increasing transmutation performance. The better neutron economy of the nitride fuel allows to design smaller ADS core and smaller spallation target which results in a much higher neutron source utilization efficiency and accordingly lower accelerator current requirements. Table 2-1 compares the major design choices and neutronic characteristics of the CERCER, CERMET and nitride cores.

2.1.4 Nuclear data issue

Additionally, problems related to evaluated nuclear data libraries problem were investigated in detail. The analysis showed that the more recent JEFF3.1 can be used as the basic library with MCB only if a correction to energy deposition is applied. The older data libraries JEF2.2 and JENDL3.3 in the release designed for burn-up calculations with MCB must be used with caution because they have significantly different behavior in standard transport (source) mode and eigenvalue calculation mode.

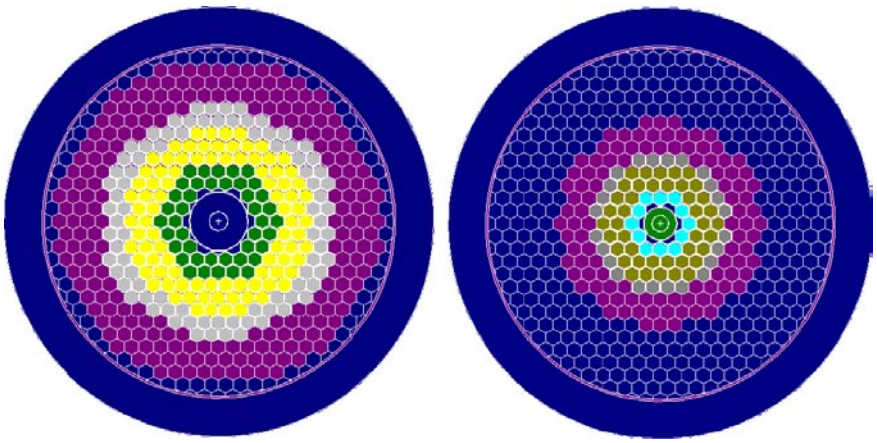

Figure 2-1. *Core maps of EFIT designs with CERMET fuel (left) and Nitride fuel (right).*

Table 2-1. Key parameters of the fuel candidates and ADS core design.

	Nitride	Cercer	Cermet
Fuel	AnN+ZrN	$AnO_{1.x}$+MgO	$AnO_{1.x}$+Mo
Coolant	LBE	Lead	Lead
Cladding steel	D9	T91	T91
Pitch to diameter ratio	1.26	1.42–1.58	1.42
Pu fraction in actinide composition, at%	41.5	47.5	46.0
Initial Keff	0.97	0.97	0.98
Reactivity swing, pcm	+100	+300	–3,500
Void worth, pcm	+3,700	+6,500	+4,800
Neutron source efficiency	1.09	0.52	0.45

2.1.5 Nitride fuel reactivity swing and power profile

Plutonium and inert matrix fractions minimising reactivity swing and power peaking factor during 3 years of operation with 145 MW thermal power were studied. The resulting Pu fraction of 41.5%, is significantly lower for the nitride core than the oxide alternatives (see Table 2-1). Suitable ZrN fractions in inner, middle and outer core zones were found to be 73.1, 68.0 and 58.4 percent volume, respectively.

2.2 Transient analysis

Transient analysis for EFIT-400 design was completed using SAS-4A for ULOF, UTOP and BT events as defined by ENEA and FZK. Cross checking of preliminarily results was made with respect to RELAP/PARCS (ENEA) and SIMMER (FZK).

A special module was constructed to simulate flow reversal through the EFIT core at the beginning of ULOF accidents in SAS4A model.

The nitride fuelled ADS design described above has been modeled by SAS4A code and the preliminary result of core's behavior under transient situation has been obtained.

Limitations to americium concentration in the fuel of fast critical reactors have been investigated using a model based on the the semi-commercial BN600 design. The safety parameters used in simulation of accidents were calculated using Monte Carlo methods (MCNP5, SERPENT) and compared to those obtained by deterministic calculations found in the literature.

2.2.1 Unprotected Loss of Flow (ULOF)

For the reason that the integrated geometry design has not been settled, the pressure drop of the first circuit was used as a paramater when studying unprotected loss of flow accidents in the EFIT-CERMET design. Results are displayed in Figure 2-2.

Comparing with results obtained by FZK using the SIMMER code, good agreement is found, except for the absence of coolant flow rate undershoot, for which a proper pump model yet had to be implemented in the SIMMER code. As shown in Figure 2-2 and 2-3, the cladding temperatures will be stable at about 1,045 K and 1,025 K for CERMET and CERCER cases correspondingly for the highest values of pressure loss. This temperature level is lower than the melting temperature of T91 but higher than the DBC-IV limit (923 K) defined in the EUROTRANS project, so the cladding failure will be the chief consequence of pin failure in ULOF transient for both CERMET and CERCER cases.

2.2.2 Unprotected over Power (UTOP)

The reference UTOP scenario is set as a linear insertion of 1,000 pcm reactivity in 0.1 seconds, according to recommendations by KIT. Thanks to the high thermal conductivity of CERMET fuel and negative net reactivity feedback, the system reaches a stable state in less than 10 seconds after the reactivity insertion, as shown in Figure 2-4. The ultimate temperature of fuel is far from its operational limit. The cladding temperature is higher than DBC-II (823 K) but lower than DBC-III (873 K).

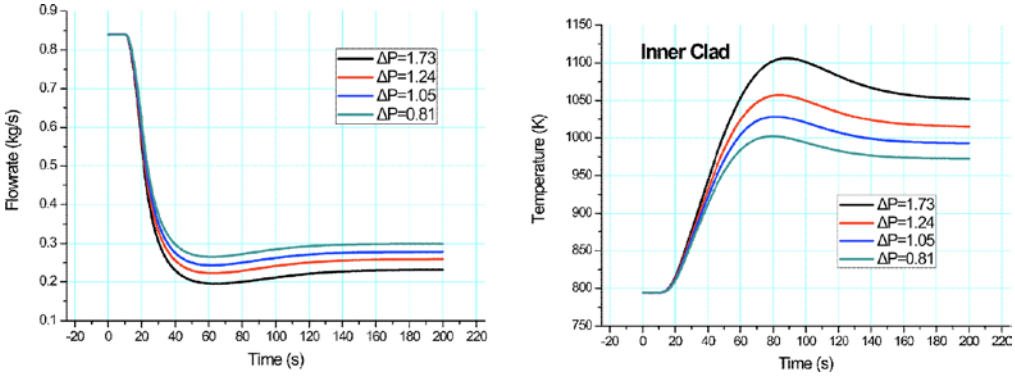

Figure 2-2. *ULOF simulation of the CERMET Fuelled EFIT Design.*

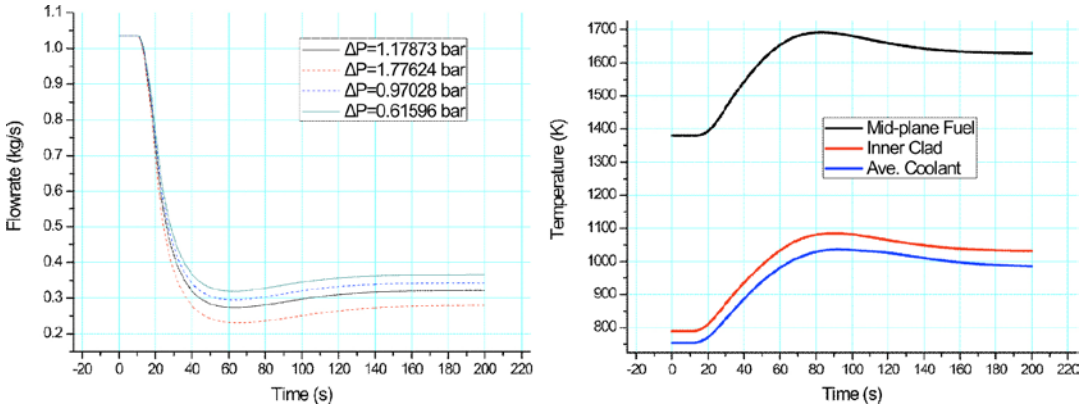

Figure 2-3. *ULOF simulation of CERCER Fuelled EFIT Design.*

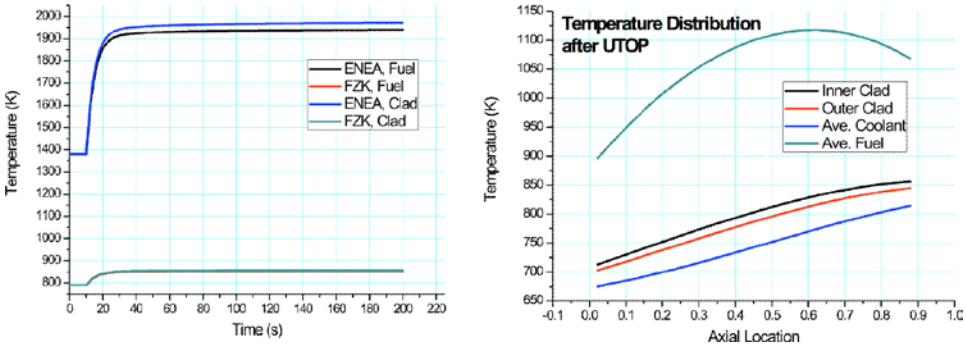

Figure 2-4. *UTOP Simulation in CERMET EFIT (Left) and CERCER EFIT (Right).*

2.2.3 Modelling of flow reversal

As found by ENEA in ULOF studies of EFIT; coolant flow reversal may result when elevations of free lead surfaces separated by pumping forces return to their original levels. At instants of zero flow, heat removal rates will be strongly reduced, and hence it is of importance to include flow reversal modelling in simulations of ULOF.

For this purpose, a two-pump model has been composed with SciLab 4.1 and integrated into SAS4A code to simulate the reverse flow caused by the elevation difference between hot pool and cold pool when the pump head is removed too fast.

In Figure 2-5, the mass flow rate through the core simulated with SAS4A using the two-pump model is compared with a RELAP/PARCS simulation performed by ENEA, showing the ability of our model to reproduce the reduction in flow rate with acceptable accuracy.

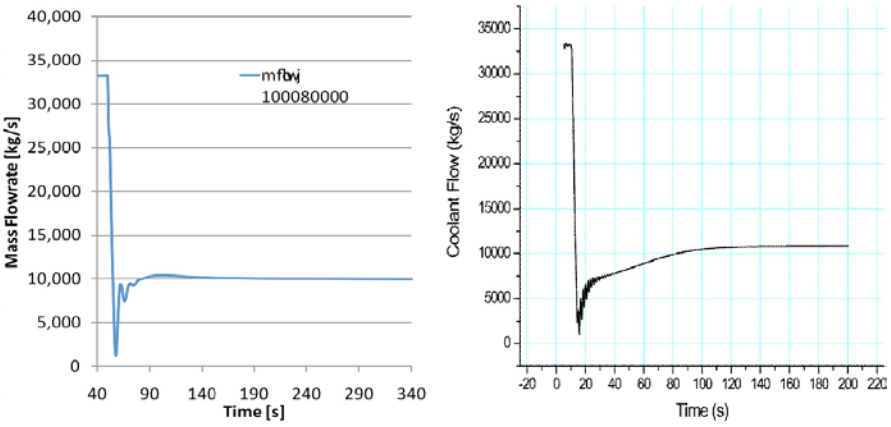

Figure 2-5. *Comparison between Two-pump Model in SAS4A (Left) and Hydraulic Model in RELAP/PARCS (Right).*

2.2.4 Limits to americium concentration in critical fast neutron reactors

The upper limit of americium that can be introduced into a medium sized sodium cooled reactor (based on the BN600 design in our case) has been estimated by accomplishing transient analysis for MOX fuel modified by different fractions of americium. The detrimental effects from americium on the safety parameters of the core has been investigated by the Monte Carlo codes MCNP5 and SERPENT, and cross-checked with the result obtained by Fazio et al using deterministic methods (VARI3D).

Table 2-2 shows first results from simulations of ULOF transients with pump coastdown half-lives of 2 and 5 seconds, and UTOP transients with reactivity insertions of 0.6 and 1.0$ at BOL. For fresh fuel, we can see that 5.9 wt% Am (8.5 wt% MA) in the fuel does not lead to coolant boiling nor fuel melting and thus may be considered as tolerable. BOL conditions are however less penalising than EOL, for which simulations will be done in 2009.

2.3 Source term

Theroretical investigations and modelling of the volatility of radiotoxic contaminants from heavy metal coolants and spallation sources have been performed in connection with the EUROTRANS, ELSY and ESS projects. Application of the thermodynamical activity parameters available from i.a. electrochemical measurements allow edus to establish upper limits for iodine, caesim, strontium and polonium volatilisation from lead-based melts (pure lead and LBE) that range several orders of magnitude below what would be expected on basis of dilution alone. Special attention has been given to issues concerning polonium, as non-thermal volatilisation from deposited condensates may complicate the issue. On the other hand, there seems to be no factual basis to the supposedly significant mechanism of volatilisation as hydride.

Table 2-2. Results from Transient Analysis in a 1,500 MWth sodium cooled fast reactor.

Am Content (%)	1.7	2.6	4.4	5.9	9.5	10.0	15.5	20.0
ULOF, $T_{1/2}$ = 2 sec.	–	Coolant Boiling	–	–	Coolant Boiling	Coolant Boiling	Fuel Melting	Fuel Melting
ULOF, $T_{1/2}$ = 5 sec	–	Coolant Boiling	–	–	Coolant Boiling	Coolant Boiling	Fuel Melting	Fuel Melting
UTOP, Δρ = 0.6 $	–	–	Fuel Melting	–	–	–	–	Fuel Melting
UTOP, Δρ = 1.0 $	–	–	Fuel Melting	–	–	Fuel Melting	–	Fuel Melting

3 Sub-criticality monitoring

During 2008 four experimental campaigns have been performed at the subcritical facility YALINA-Booster in Minsk, Belarus. The main objective is the qualification of reactivity monitoring techniques as well as to develop the electronic chains that can be used in a power ADS. The work has been carried out within the framework of the EUROTRANS project domain 2 which is a part of the 6th framework program /1/. For this purpose four different subcritical configurations have been studied during 2008:

1. March 2008: Configuration SC0 (k_{eff}~0.977)
2. June 2008: Configuration SC3a (k_{eff}~0.95)
3. October 2008: Configuration SC3b (k_{eff}~0.95)
4. November 2008: Configuration SC6 (k_{eff}~0.85)

Some of the results from configuration SC3a are presented below.

3.1 Experimental set-up

The YALINA-Booster is a subcritical fast-thermal core coupled to a neutron generator. The neutron generator uses a deuteron ion accelerator impinging on a TiT or TiD target to produce fusion neutrons. With a diameter of 45 mm, the target is located in the centre of the core. In the experiments presented here only the Ti-T target was used, thus providing a quasi-isotropic neutron energy spectrum of 14 MeV. The neutron generator can be operated in both continuous and pulse modes and gives thereby the possibility of performing both pulsed neutron source (PNS) measurements and continuous wave measurements. Moreover, the continuous wave can be promptly interrupted (~1 μs) followed by a fast beam restart. In this way, short repeated beam trips can be induced intentionally with interruption times in the millisecond scale. The maximum beam current in continuous mode is around 1.5 mA giving a maximum neutron yield of approximately 10^{11} neutrons per second.

The core /2/, depicted in Figure 3-1, consists of a central lead zone (booster), a polyethylene zone, a radial graphite reflector and a front and back biological shielding of borated polyethylene. The booster zone has been loaded with two different arrangements of 36% enriched UO_2 pins while the polyethylene is loaded with 10% enriched UO_2 fuel pins. The SC3a configuration presented here is based on 1077 fuel pins, 10% enriched and has a k_{eff} ~0.95.

The fast-spectrum lead zone and the thermal-spectrum polyethylene zone are separated by a so called thermal neutron filter, or valve zone, consisting of one layer of 108 pins with metallic natural uranium and one layer of 116 pins with boron carbide (B_4C), which are located in the outermost two rows of the fast zone. Hence, thermal neutrons diffusing from the thermal zone to the fast zone will either be absorbed by the boron or by the natural uranium. In this way, a coupling of mainly fast neutrons between the two zones is maintained.

The three B_4C-control rods that can be inserted in the thermal zone have allowed us to slightly change (–0.5$) the reactivity of the system. Hence, the sensitivity of the different reactivity monitoring techniques can be tested.

There are seven axial experimental channels (EC1B–EC4B and EC5T–EC7T) in the core, two axial (EC8R and EC9R) and two radial experimental channels (EC10R and EC11R) in the reflector. In addition, there is one neutron flux monitoring channel in each corner of the core (MC1–4) and outside the reactor (not shown in the figure).

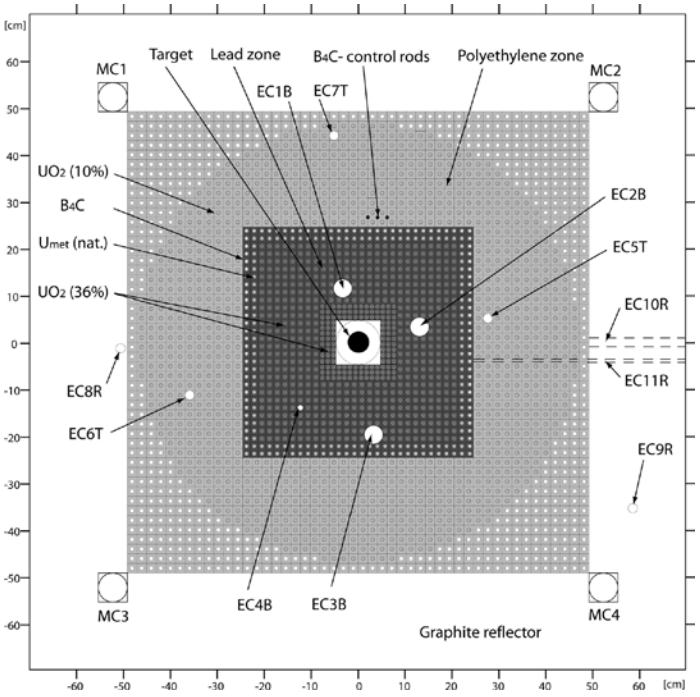

Figure 3-1. *Schematic cross-sectional view of the YALINA reactor core for the SC3a configuration.*

3.2 Pulse neutron source experiments

In the pulsed neutron source (PNS) experiments, the kinetic evolution of the system is measured after the repetitive injection of a neutron pulse. Two methods have been used to obtain the reactivity from the PNS measurements: the area method /3/ (also referred as the Sjöstrand method) and the determination of the prompt decay constant /4/.

Figure 3-2 shows the kinetic evolution of the neutron flux measured at different locations of the reactor to a neutron pulse of 5 μs with a repetition rate of 50 Hz. Inspecting the figure we can observe the different evolutions obtained at the booster (EC1B) or the innermost thermal zone (EC5T), which present a fast decay during the first millisecond followed by a slow decay, compared with the evolution at the graphite reflector (MC2) or outside the reactor (Y.T.), which increase the level over the first two milliseconds to decay slowly afterwards. It must be pointed out that in order to reduce statistical uncertainties it has been necessary to accumulate the kinetic response from a large number of pulses. In addition, due to the high counting rates observed in some of the detectors, it was necessary to take into account the effect of the dead time, leading to corrections in the peak amplitude up to 25% for the highest intensities.

3.2.1 Prompt decay constant method

From the point kinetic approximation, we find that the kinetic evolution of prompt neutrons after a pulse follows an exponential decay with decay constant, α:

$$\alpha = \frac{\rho - \beta_{eff}}{\Lambda} \quad \text{or} \quad \frac{\rho}{\beta_{eff}} = \frac{\alpha}{\beta_{eff}/\Lambda} + 1$$

where ρ is the reactivity, β_{eff} the effective delayed neutrons fraction and Λ the mean neutron generation time. Hence, if the value β_{eff}/Λ is known, the value of ρ (in units of β_{eff}) can be calculated. The value of $\beta_{eff}/\Lambda = 114 \pm 2\ s^{-1}$ has been obtained from MCNP calculations. With this constant, the values of the reactivity obtained with the slope fit method are shown in Table 3-1.

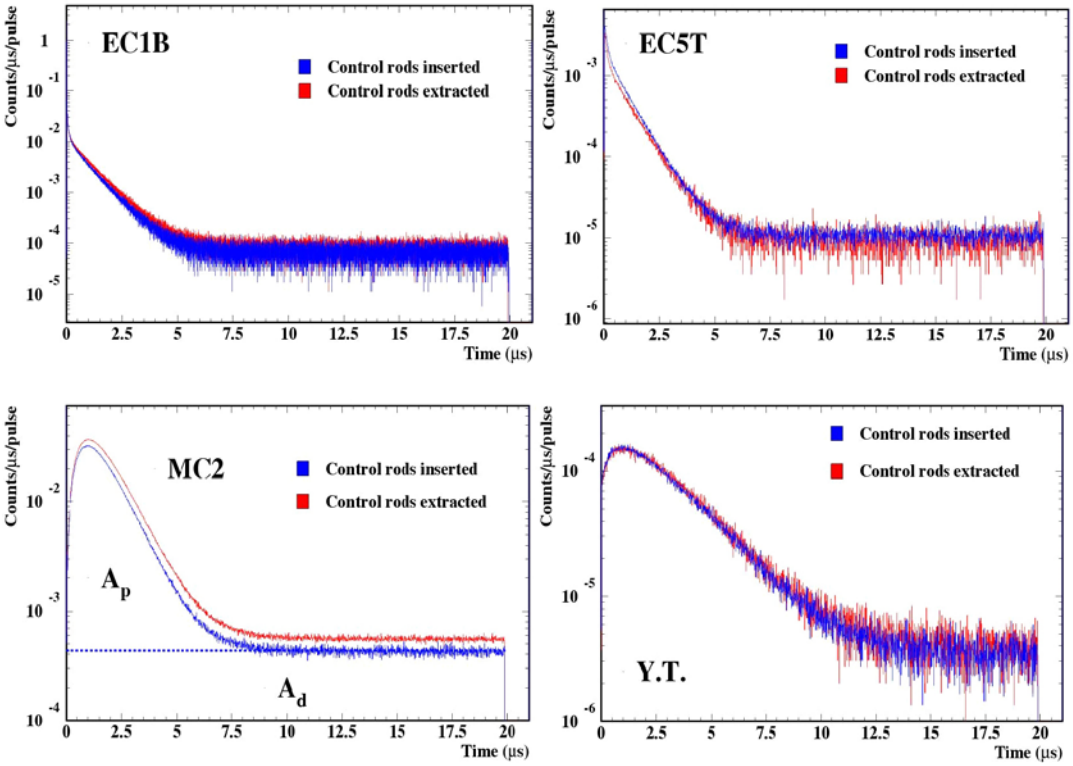

Figure 3-2. *Kinetic evolution of the neutron flux measured at different locations in YALINA SC3a configuration to a 5 µs pulse repeated at 50 Hz. The plots show accumulated statistics for about 10^5 neutron pulses.*

Table 3-1. Reactivity values obtained from the prompt decay constant for different regions of the reactor. The measurements were performed with the control rods inserted and extracted.

		Control rods extracted		Control rods inserted	
		α (s–1)	ρ ($)	α (s–1)	ρ ($)
Booster zone	**EC1B**	–1,026 ± 17	–7.97 ± 0.19	–1,096 ± 21	–8.58 ± 0.22
	EC2B	–	–	–1,087 ± 16	–8.50 ± 0.19
	EC3B	–	–	–1,090 ± 4	–8.53 ± 0.13
Thermal zone	**EC5T**	–1,031 ± 26	–8.01 ± 0.26	–1,107 ± 37	–8.68 ± 0.34
	EC6T	–	–	–1,089 ± 15	–8.52 ± 0.18
Graphite reflector	**MC2**	–976 ± 6	–7.53 ± 0.12	–1,018 ± 8	–7.89 ± 0.14

3.2.2 Area method

The area method states that the reactivity, in dollars, can be determined as follows:

$$\frac{\rho}{\beta} = -\frac{A_p}{A_d} = 1 - \frac{A_t}{A_d}$$

where A_p is the area under the pulse that is due only to the prompt neutrons generated after the pulse; A_d the area due only to the delayed neutrons, and A_t is the total area under the curve, as shown in the bottom-left panel of Figure 3-2.

Table 3-2 shows the area method reactivity values in the different detectors. Inspecting the table we can observe large differences among detectors located in the booster and the thermal or reflector zones. These differences arise from the different positions relative to the neutron source and the different neutron absorption cross section in the different reactor regions and close to the detectors. Nevertheless we observe that the reactivity reaches a stable value when the distance from the detector to the neutron source is large enough.

Table 3-2. Reactivity values directly obtained with the area method from different detectors. The measurements were performed with the control rods inserted and extracted.

		Control rods extracted	Control rods inserted
Booster zone	**EC1B**	–14.93 ± 0.17 $	–17.17 ± 0.22 $
	EC2B	–	–15.30 ± 0.15 $
	EC3B	–	–10.18 ± 0.04 $
Thermal zone	**EC5T**	–8.77 ± 0.35 $	–9.46 ± 0.21 $
	EC6T	–	–7.57 ± 0.14 $
Graphite reflector	**MC2**	–7.26 ± 0.03 $	–7.88 ± 0.06 $
	MC3	–7.33 ± 0.96 $	–7.96 ± 1.13 $

3.2.3 Beam-Trip Measurements

A current-to-flux relation technique for reactivity monitoring can only provide relative measurements of the reactivity. Therefore, it is necessary to use absolute reactivity determination techniques to calibrate the former technique. To limit the perturbation to the power operation of ADS, we can take profit from the unavoidable occurrence of beam trips or imposed beam trips.

The source jerk technique is based on the determination of the kinetic parameters after removal of the prompt neutron source, in analogy to the rod-drop technique /5/. The main advantage of this technique is related to the fact that no fitting, based on an interpretation model, must be performed. On the other hand, corrections may be needed to take into account energy and spatial effects.

In order to reduce statistical uncertainties we have averaged several beam trips, as presented in Figure 3-3. This procedure has also allowed us to obtain a good estimation of the prompt decay constant. Inspecting the figure, we can see (in the left panel) the results of a beam trip with the insertion or extraction of the control rods. Comparing these results with the results of the area method, we can observe that the source jerk technique provides similar values. On the other hand, if we observe the right panel we can estimate the prompt decay after subtracting the delayed neutron level. It is possible to see that the decay is different when we insert or extract the control rods, leading us to detect small variations of the reactivity.

3.2.4 Conclusions

The experimental results obtained during the SC3a phase of the EUROTRANS experiments at the YALINA-Booster facility have been presented. The main objective has been to demonstrate the possibility of monitoring the reactivity of the system using short beam trips.

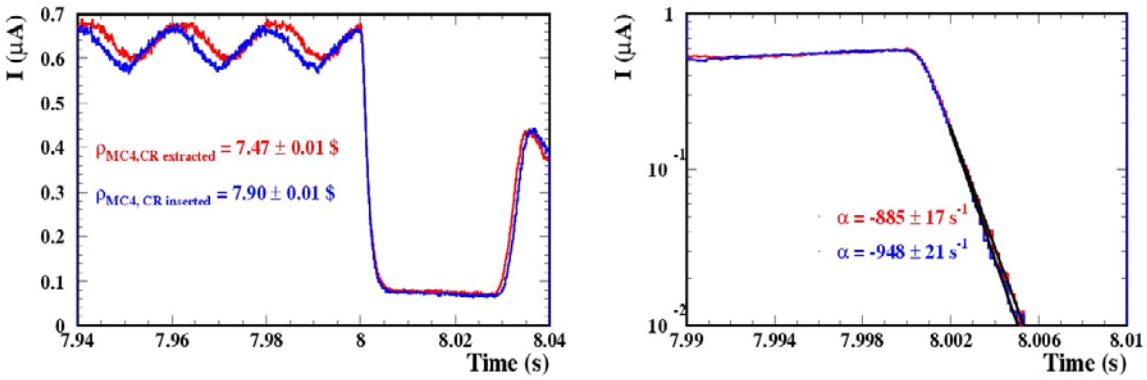

Figure 3-3. *Averaged beam trip sequence with control rods inserted and extracted. (Left panel) Source jerk technique. (Right panel) Delayed neutron level has been subtracted to estimate the different decay constant.*

Using PNS techniques, we have obtained the reference reactivity values for each detector and it was observed that the results carry strong spatial effects.

It was shown that the beam trip technique can be used to obtain the reactivity at beam trips and the values can be used for calibration of a current-to-flux reactivity indicator.

3.3 Neutron detection at YALINA-booster

As described above, the YALINA-Booster facility is a two-zone sub-critical core coupled to a neutron source. The inner fast zone is closely packed to the neutron source while the thermal zone surrounds the fast zone.

The experimental part of the YALINA-Booster project experienced a boom in 2008. At the same time, data analysis and evaluation of previously-obtained data was ongoing. Monte Carlo simulations (MCNP) of the core were performed. One group of the calculations focused on simulation of the periphery flux measurements by ^{3}He detectors. The calculations were performed for two different configurations and the results were cross-checked with the experimental values resulting in good agreement. Even fine details of the obtained flux distribution could be explained utilizing further MCNP calculations.

Besides the periphery flux investigation, also measurements of the fast part of the neutron spectrum were compared with MCNP calculations. Namely the multiple foil activation technique results were compared with simulations using reaction rates. The experimental reaction rate, R^{exp}, was defined as follows:

$$R^{exp} = S\,\lambda\, e^{-\lambda t_c}\,(1-e^{-\lambda t_m}) / K\,(1-e^{-\lambda t_a})\,A_r\,m\,N_A,$$

where S is the net peak area, λ is the decay constant of the activation product, t_a is the time of activation, t_c is the time of cooling, t_m is the time of measurement, ε is the simulation-based correction factor (see below), K is the isotopic abundance in the foil material, A_r is the mass number, m is the foil mass and N_A is the Avogadro constant. The comparison revealed a problem with the number of source neutrons which was a result of another experiment. Besides that, high uncertainties in lead cross-sections were observed.

Another group of the YALINA-Booster calculations aimed for comparison of calculated and measured neutron flux distribution in the radial direction. This experiment took into account only thermal and epithermal neutron flux. The comparison confirmed conclusions obtained for the fast spectrum. Some of the above mentioned results together with further calculations (as an example see Figure 3-4 below) were submitted to Nuclear Instruments and Methods in Physics Research, section A.

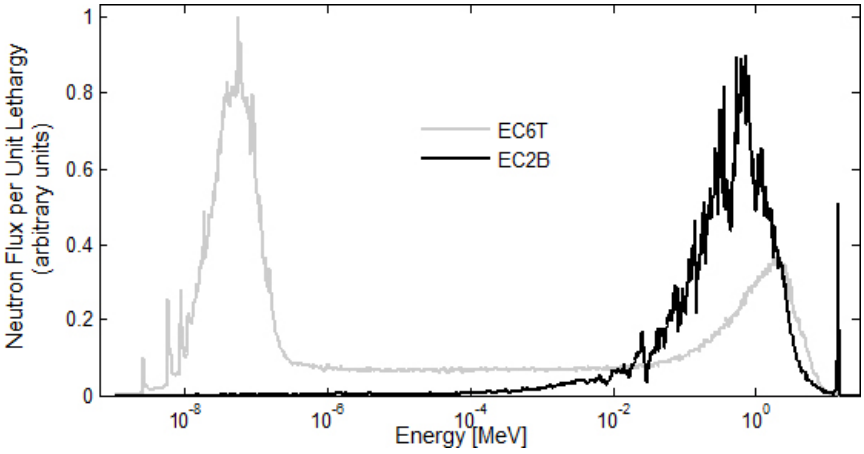

Figure 3-4. *Neutron spectrum inside experimental channels located in the thermal (EC6T) and booster (EC2B) zone (calculated by MCNP).*

3.4 Deviations from point kinetics

The ADS approach raises a problem of searching robust methods for reactivity monitoring of subcritical facilities for safe operation of such installations. The YALINA experiment in Belarus is designed to answer this demand. It has become common to use the Pulsed Neutron Source (PNS) technique to measure the criticality level. In doing so, one usually assumes the point kinetics behavior of the system in question. This assumption works very well for the critical reactors but it is sometimes questionable for subcritical facilities. For example, 3-5 presents two sharply different detector responses collected at two different locations.

As seen in the picture, one of the signals has a peak whereas the other does not.

In an attempt to explain this peculiarity, a simple diffusion model with delayed neutrons was considered. More specifically, it was assumed one prompt and one average delayed neutron group in the infinite slab geometry.

$$\begin{cases} \dfrac{1}{v}\dfrac{\partial\Phi(x,t)}{\partial t} = D\dfrac{\partial^2\Phi(x,t)}{\partial x^2} + \left[(1-\beta)\nu\Sigma_f - \Sigma_a\right]\Phi(x,t) + \lambda C(x,t) \\ \dfrac{\partial C(x,t)}{\partial t} = \beta\nu\Sigma_f\Phi(x,t) - \lambda C(x,t) \end{cases}$$
$$-\infty < x < \infty, \quad 0 \le t < \infty$$

The solution to this equation was found to be

$$\phi(z,\tau) = \frac{1}{2l\sqrt{\pi\tau}}e^{-\tau-\frac{z^2}{4\tau}} - \frac{2\xi}{\sqrt{\pi}\gamma^2}\sqrt{\tau}\,e^{-\tau-\frac{z^2}{4\tau}} + \frac{\xi}{2\gamma^3}e^{-\lambda m\tau} \times$$
$$\times\left[e^{-\gamma z}(\gamma z+1)\operatorname{erfc}\left(\frac{z}{2\sqrt{\tau}}-\gamma\sqrt{\tau}\right) + e^{\gamma z}(\gamma z-1)\operatorname{erfc}\left(\frac{z}{2\sqrt{\tau}}+\gamma\sqrt{\tau}\right)\right]$$

Here, z and τ are scaled space and time variables that are related to the original variables, x and t, through

$$x = l\cdot z, \quad t = m\cdot\tau, \quad \Phi = \eta\cdot\phi$$

Here, the scaling factors, l, m and η, are

$$l = \frac{L}{\sqrt{1-k_\infty}}, \qquad m = \frac{\tau_a}{1-k_\infty}, \qquad \eta = l.$$

They are expressed through the diffusion length, L, mean free time, τ_a, and multiplication factor of an infinite homogeneous system, k_∞. These parameters are given as usual

$$L^2 \equiv \frac{D}{\Sigma_a}, \quad k_\infty \equiv \frac{\nu\Sigma_f}{\Sigma_a}, \quad \lambda_a \equiv \frac{1}{\Sigma_a}, \quad \tau_a \equiv \frac{\lambda_a}{v}$$

In addition, it was found that the location of a pulse's pick, z, and the time, τ, when the pick arrives at the location z are related to each other as

$$z^2 = 2\tau(1+2\tau)$$

Figure 3-6 presents several plots of the obtained solution.

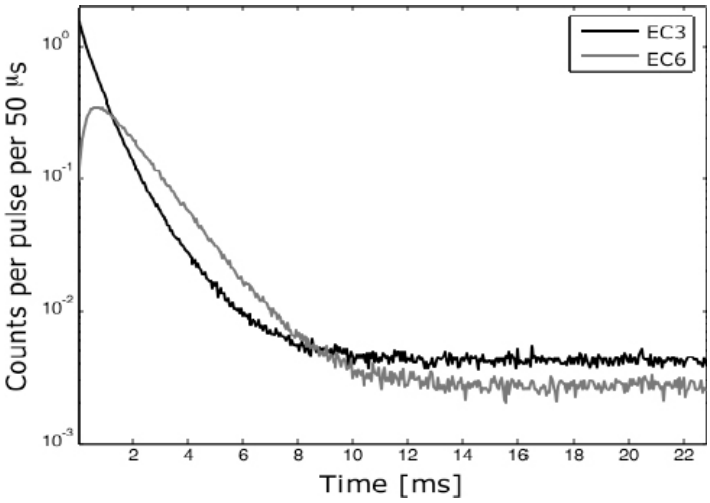

Figure 3-5. *Experimental data from two different detectors.*

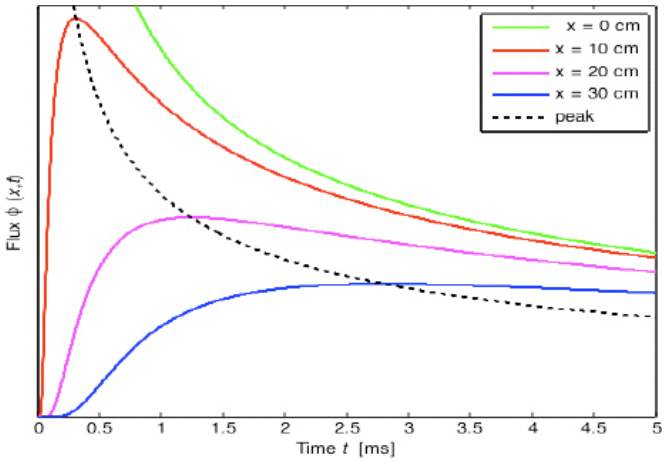

Figure 3-6. *Time behaviour of the solution at several locations.*

By varying detector location, we see that the neutron flux decreases with increasing the distance from the source (which is assumed to be at the origin, x = 0). This property is expected on physical grounds. In same way, the pulse peak decreases exponentially with increasing the detection position, black curve shows how the flux peak develops in time, furthermore, the time delay increases when the detector moves away from the source. It is seen that the solution close to the origin has a non-peaked shape typical for detectors situated close to the neutron source. What is more important the analytic solution represents peaked signals as well, as seen in Figure 3-6. It gives grounds to believe that the derived analytical solution may turn out to be promising to explain and extract the reactivity and other important parameters from detector readings.

4 Fuel modelling

4.1 Introduction

Among the fuels suggested for transmutation purposes are the CERMET and CERCER fuels. The former consists of actinide dioxides enclosed in a metal matrix and the latter of actinide dioxides enclosed in a ceramic matrix. For the CERMET fuels molybdenum has been selected as matrix material and for the CERCER fuels magnesium oxide is the most promising candidate /6/. As these fuels are intended for transmutation purposes the concentration of minor actinides in the fuel will be high and thereby the alpha activity of the fuel phase, this is mainly due to the decay of americium and curium in the fuel. Therefore, the understanding of the behaviour of helium in these matrices is important from a fuel performance perspective. So far some experimental work has been conducted on helium diffusion in these matrix materials the results show that helium tends to form bubbles in vacancy defect and are at certain temperatures released in parts to the surroundings /7/. These experimental results give satisfactory data for qualitative discussions, but for modelling efforts more intrinsic knowledge on the atomistic behaviour is needed.

Our goal has therefore been to use first principle calculations to calculate not only the binding energies of helium to these bubble formations but also kinetic parameters needed to model the temperature behaviour of these non reversible processes.

4.2 Methodology

In this work we have used standard calculations within the density functional theory (DFT) to calculate binding energies and vibrational frequencies. This is done by use of the Vienna Ab initio Simulation Package (VASP). So far only calculations for helium bubble formation in molybdenum has been conducted. This system was chosen as a starting point for the existence of well controlled experiment conducted on molybdenum single crystals. The aim has been to develop a methodology possible to extend into the magnesium oxide system and beyond.

In this work a super cell containing 128 molybdenum atoms was used as bulk material and with the GGA potentials supplied by the VASP group /8/, the formation energy of helium bubbles formed in vacancies was calculated according to

$$\Delta E_f(He_nV_1) = E(He_nV_1) - (127/128)\cdot E(Mo) - n\cdot E(He)$$

where ΔE_f is the formation energy of a given configuration and E is the total energy as calculated by the code. E(He) is the energy of a free helium atom, calculated to be 0.0131 eV and E(Mo) is the cohesive energy of the reference state.

This together with the formation energy of interstitial helium atoms in molybdenum made it possible to calculate the binding energy of helium atoms to these bubbles.

Using the harmonic oscillation approximation /9/ vibrational frequencies was calculated for helium atoms in the bubbles. These together with the binding energies of the bubbles give the release frequency of helium atoms from the bubbles into the surrounding molybdenum crystal from /10/:

$$\Gamma = \upsilon \cdot e^{\Delta E/k_B T}$$

where υ is an effective frequency associated with the vibration of the helium atom, ΔE the binding energy of a helium atom, k_B the Boltzmann constant and T the absolute temperature.

Denoting small helium bubbles with He_nV_m, and an interstitial helium atom with I, the previous assumption, derived from experimental results, has been that the helium release from clusters can be described by the following reaction:

$$He_nV_1 \rightarrow He_{n-1}V_1 + I$$

Using this, the helium release from the bubbles can be modeled using rate theory /10/ where the time evolution of helium bubbles of a certain size can be assumed to take the following form:

$$\frac{dn_i}{dt} = \Gamma_{i+1} - \Gamma_i$$

4.3 Results

Using the methods described above, helium binding energies and vibrational frequencies were calculated and are given in Table 4-1.

With this data the state evolution of helium bubbles was modelled and the results are depicted in Figure 4-1. From these it is possible to reproduce the desorption spectrum, which is the original experimental results used to derive the results presented above. Such a spectrum is presented in Figure 4-2. Both these figures also includes the experimental data and are for a single molybdenum crystal filled with helium, as it is being heated with a heating rate of 10 K/s. Thereby the temperature scale can also be seen as the time scale of the experiment.

Table 4-1. Formation energies and vibrational frequencies.

	ΔE (eV)			υ(s^{-1})		
State	**This work**	**Ref. /11/**	**Ref. /12/**	**This work**	**Ref. /11/**	**Ref. /12/**
He_5V_1	2.00	2.11	2.32	$1.9 \cdot 10^{13}$	$0.7 \cdot 10^{13}$	$6.2 \cdot 10^{14}$
He_4V_1	2.54	2.4	2.7	$1.6 \cdot 10^{14}$	$3 \cdot 10^{13}$	$5.3 \cdot 10^{15}$
He_3V_1	2.54	2.6	2.61	$2.3 \cdot 10^{13}$	$5 \cdot 10^{13}$	$2.3 \cdot 10^{14}$
He_2V_1	2.67	2.9	2.8	$1.9 \cdot 10^{13}$	$3.0 \cdot 10^{14}$	$1.4 \cdot 10^{14}$
He_1V_1	3.64	3.8	3.75	$7.6 \cdot 10^{13}$	$5.0 \cdot 10^{15}$	$3.0 \cdot 10^{15}$

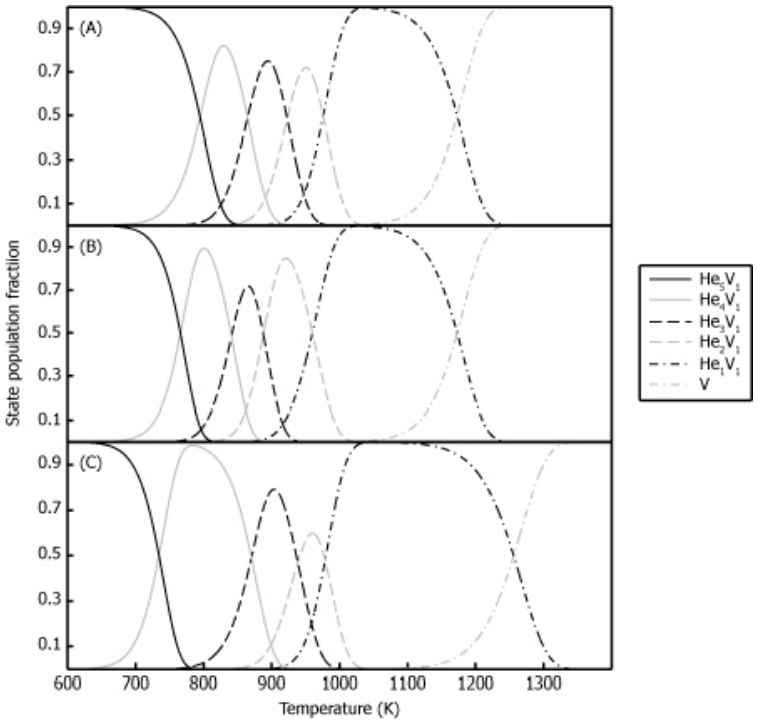

Figure 4-1. *State evolution for helium bubbles (A) ref. /11/, (B) ref. /12/ and (C) this work.*

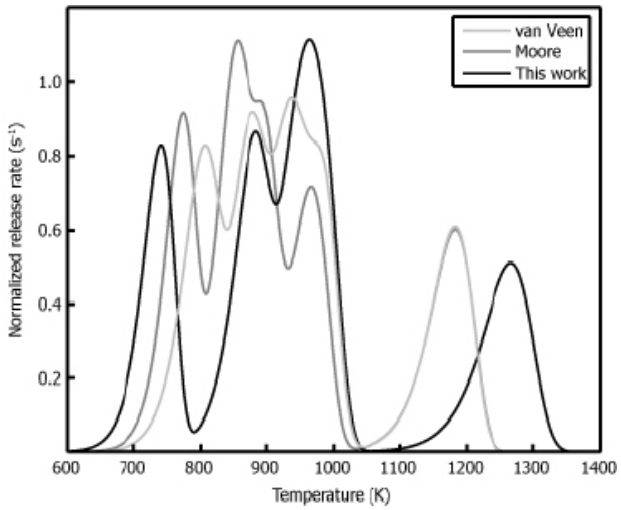

Figure 4-2. *Helium release rates, first principal results compared with experimental results.*

4.4 Conclusions

As seen from the results in Figure 4-1 and 4-2, the state evolution and helium desorption spectrum is reproduced with good accuracy except in the high temperature regime. The discrepancy at higher temperatures is most likely attributed to model errors. At these temperatures the helium self diffusion rate starts to be significant and this could lead to other diffusion paths than assumed from the previous experimental works.

However, apart from this the helium retention in molybdenum vacancies are modelled with a high degree of accuracy. This indicates the possibility to use the same methodology for helium bubble formation and diffusion in other systems as well, at least for moderate temperatures.

4.5 Fuel laboratory

A new fuel laboratory has been established at the KTH Campus for the manufacture of various types of uranium-containing powders and pellets. The presently available equipment allows high-temperature synthesis, milling, mixing, pressing and sintering of powders as well as XRD, SEM, thermogravimetric and mechanical analysis of the produced materials. The production of high-quality uranium nitrides by sequential hydriding and nitriding of uranium metal and inert additives has been proven to work as intended. Figure 4-3 shows a photo of the laboratory in its early stage of construction.

Figure 4-3. *The uranium fuel laboratory at KTH.*

5 Modelling of radiation damage in steels

The useful properties of steels are due to a complicated microstructure containing iron and chromium carbides. Only some basic physical properties of these carbides are known with high precision, although the carbides may have a vital impact on the performance and longevity of the steel. To improve on this situation, we performed extensive density-functional theory calculations of several carbides. The quantitative results were in perfect agreement with the relative empirical stability of the carbides. Also, in contradiction with experimental data, we find that $Cr_{23}C_6$ responsible for the hardness of stainless steels is not the most stable chromium-dominated carbide. The results were published in Applied Physics Letters.

In addition, to understand the behaviour of dissolved carbon in iron and chromium, first-principles density-functional theory calculations for carbon solution enthalpies, and diffusion activation enthalpies, in body-centered-cubic Fe and Cr were performed. The results for C in Fe compare well with experiments, provided that the effect of magnetic disordering is accounted for. Likewise, in Cr, the calculated solution and diffusion activation enthalpies agree well with available experiments. In both materials, the deviation between calculated enthalpies and critically assessed experimental enthalpies are less than 0.05 eV. Further, first-principles calculations for the interaction energies between a solute (e.g. a Cr atom in bcc Fe) and an interstitial C atom were obtained. The results are in conflict with those inferred from internal friction (IF) experiments in disordered Fe-Cr-C alloys. A simple model of C relaxation in disordered Fe-Cr is used to compare theoretical and experimental IF curves directly, suggesting that a more extensive study of the energetic, thermodynamic, and kinetic aspects of C migration in Fe-Cr is needed. These results were published in Physical Review B.

6 References

/1/ **Knebel J, Abderrahim H A, Cinotti L, Delage F, Fazio C, Giot M, Giraud B, Gonzalez E, Granget G, Monti S, Mueller A C, 2006.** European Research Programme for the Transmutation of High Level Nuclear Waste in an Accelerator Driven System, FISA 2006.

/2/ **Kiyavitskaya H (coordinator), 2007.** YALINA-Booster Benchmark Specifications for the IAEA Coordinated Research Projects on Analytical and Experimental Benchmark Analysis on Accelerator Driven Systems and Low Enriched Uranium Fuel Utilization in Accelerator Driven Sub-Critical Assembly Systems, IAEA.

/3/ **Sjöstrand N G, 1956.** Measurement on a subcritical reactor using a pulsed neutron source, Arkiv för fysik 11, 13.

/4/ **Simmons B E, King J S, 1958.** A Pulsed Technique for Reactivity Determination, Nucl. Sci. Eng. 3, 595.

/5/ **Keepin G R, 1965.** Physics of Nuclear Kinetics, Addison Wesley Publishing Company INC, USA.

/6/ **Maschek W, Chen X, Delage F, Fernandez-Carretero A, Haas D, Matzerath Boccaccini C, Rineiski A, Smith P, Sobolev V, Thetford R, Wallenius J, 2008.** Prog. Nucl. Energy, 50, 333–340.

/7/ **Van Veen A, Konings R J M, Fedorov A V, 2003.** J. Nucl. Mater., 320, 77–84.

/8/ **Kresse G, Joubert D, 1999.** Phys. Rev. B, 59, 1758.

/9/ **Ashcroft N W, Mermin N D, 1976.** Solid State Physics, Harcourt College Publishers.

/10/ **Vineyard G H, 1957.** J. Phys. Chem. Solids, 3, 121–127.

/11/ **van Veen A, Evans J H, Th W, Buters M, Caspers L M, 1983.** Radiat. Eff., 78, 53–66.

/12/ **Moore W T, Kornelsen E V, 1985.** Radiat. Eff., 90, 141–147.

7 List of publications

Persson C-M, Fernández-Ordóñez M, Villamarín D, Bécares V, González-Romero E M, Bournos V, Serafimovich I, Mazanik S, Fokov Y, Kiyavitskaya H, 2008. Pulsed neutron source measurements in the subcritical ADS experiment YALINA-Booster, Annals of Nuclear Energy 35, 2357–2364.

Wallenius J, Westlen D, 2008. Hafnium clad fuels for fast spectrum BWRs. Annals of Nuclear Energy 35, 60.

Sandberg N, Henriksson K, Wallenius J, 2008. Carbon impurity dissolution and migration in bcc Fe-Cr. Physical Review B 78, 094110.

Henriksson K, Sandberg N, Wallenius J, 2008. Carbides in stainless steels – results from ab initio investigations. Applied Physics Letters 93, 191912.

Harari N, 2008. Subcritical Reactor Response to a Neutron Pulse, Master of Science thesis, KTH, Stockholm.

Morra E, 2008. Transmutation of nuclear waste in a boiling water reactor with hafnium clad M.Sc. Thesis, Division of Reactor Physics, KTH.

Note: Carl-Magnus Persson has during 2008 changed his name to Carl Berglöf.

8 List of participation in conferences and project meetings

Andrei Fokau

- EUROTRANS ITC-6 School, Madrid, Spain, April 5–12

Calle Berglöf

- EUROTRANS ECATS meeting in Aix-en-Provence, France, January 28–February 02
- IAEA Workshop on Neutron Fluctuations in Reactors, Trieste, Italy, September 21–26

Mikael Jolkkonen

- Asia-Link Summer School, Beijing, China, June 22–26
- CONFIRM, final meeting, Petten, August 21–22
- ELSY WP 2 meeting, Genoa, September 23–24
- ESS WP 9.1 meeting, Zürich, November 26–27

Odd Runevall

- OECD information exchange meeting on P&T, Mito, Japan, October 6–10.

Milan Tesinsky

- EUROTRANS/ECATS meeting, Aix-en-Provence, France January 30–31.
- IP-EUROTRANS Internal Training Course ITC6, Madrid, Spain, April 2–5.
- World Nuclear University – Summer Institute, Ottawa, Canada, July 5–August 16.
- OECD exchange meeting on P&T, Mito, Japan, October 6–10.

Janne Wallenius

- EUROTRANS DESIGN meeting, Genoa, Italy, April 2–3
- EUROTRANS Governing Council meeting, Brussels, Belgium, April 17
- Asia-Link board meeting in Beijing, China, April 28–29.
- EUROTRANS WP1.5 meeting in Bologna, Italy, May 29–30
- ANS summer meeting in Anaheim, USA, June 11–13
- Asia-Link Summer school in Beijing, China, June 23–27
- CONFIRM-meeting in Petten, The Netherlands, August 21–22
- PATEROS-meeting in Paris, France, August 28–29
- EUROTRANS DEMETRA meeting, Barcelona, Spain, September 15–17
- EUROTRANS DESIGN meeting, Karlsruhe, Germany, September 30–October 1st
- ELSY Governing Council meeting, Karlsruhe, Germany, October 2nd
- OECD information exchange meeting on P&T, Mito, Japan, October 6–10.
- Asia-Link final meeting, Beijing, China, October 29–30.
- EUROTRANS WP1.5 meeting in Karlsruhe, Germany, November 27–28.

Youpeng Zhang

- EUROTRANS ITC-6 School, Madrid, Spain, April 5–12
- VELLA Thematic School, Karlsruhe, Germany, November 12–14.